II. *Mariner* Venus–Mercury 1973 Project

A. Project Description

The *Mariner* Venus–Mercury 1973 Project was authorized in December 1969. The primary objective of this first dual-planet mission is to conduct exploratory investigations of the planet Mercury's environment, atmosphere, surface, and body characteristics, and to obtain environmental and atmospheric data on the planet Venus (first priority assigned to Mercury investigations). The secondary objectives are to perform interplanetary experiments enroute to Mercury, and to obtain experience with the gravity-assist mission mode.

A single *Mariner* spacecraft is planned for launch by an *Atlas/Centaur* vehicle from Cape Kennedy in October 1973. The Venus encounter, in February 1974, will provide both an opportunity to obtain scientific data at that planet and the necessary energy, by means of gravity-assist, to reach Mercury some 7 wks later. The spacecraft design is expected to resemble that used in the *Mariner* Mars 1969 mission and that being developed for the *Mariner* Mars 1971 mission, with appropriate modifications defined by the Venus–Mercury mission requirements. The scientific experiments, which include television and other planet-oriented elements together with interplanetary fields-and-particles investigations, were selected by NASA Headquarters during July 1970. These experiments are listed in Table 1, along with the corresponding Principal Investigators and Science Team Leaders. The Deep Space Network and other NASA facilities will be committed to support the mission. It is planned that a System Contractor will be selected in early 1971. The Contractor's effort would encompass the spacecraft detail engineering, system assembly, test and operations, and selected support to other elements of the Project.

Table 1. Experiments and principal investigators

Experiment	Principal Investigator	Affiliation
Celestial Mechanics–Radio Science	H. T. Howard[a]	Stanford University
Charged-Particle Telescope	J. A. Simpson	University of Chicago
Infrared Radiometer	S. C. Chase	Santa Barbara Research Corp.
Magnetic Fields	N. F. Ness	Goddard Space Flight Center
Plasma Science	H. S. Bridge	Massachusetts Institute of Technology
Television Science	B. C. Murray[a]	California Institute of Technology
Ultraviolet Spectroscopy	A. L. Broadfoot	Kitt Peak National Observatory

[a]Science Team Leader.

B. Imaging Experiment, *Space Photography Section*

1. Introduction

The objectives of the imaging experiment are to: map and identify the major physiographic provinces of Mercury on the basis of topographic forms and optical properties of surface materials; determine the similarities and differences between the major surface features of Mercury and those on the earth, the moon, and Mars, with special emphasis on the recognition of endogenic structures; determine the distribution of surface features with reference to the dynamic axes of Mercury and investigate the boundaries with surrounding terrain; and establish correlations with earth-based observations. For the planet Venus close-up photography will produce additional spectral, radio emission, and radio occultation observations.

2. Exploration of Mercury

a. Morphology of local features. Topographic and size distribution of craters will be investigated for age implications and comparisons with slopes and shapes of lunar craters. Search will be made for evidence of nonlunar processes, latitudinal and longitudinal topographic variations, impact features, topographic forms with possible implications of unusual endogenic phenomena, and possible nonlunar and non-Martian features.

b. Cartography and geodesy. In conjunction with earth-based radar data and radio occultation data from the spacecraft, the television data will determine whether or not the planet departs significantly from a spherical shape. Also, the orientation of the spin axis of the planet will be determined with greater precision than currently possible from earth. These results combined with images of the surface features will be used to establish a coordinate system and to produce a map.

c. Photometric properties of local features. Rayed craters and other phenomena showing different albedos and photometric functions from surrounding areas will be searched. Attention will be given to the possibility of an exogenic darkening process and its effect on the optical properties of Mercury, the moon, and the Galilean satellites. The morning terminator will be searched for evidences of transitory frosts and the evening terminator for evidence of fluorescence. Attempts to establish correlations with earth-based radar observations will be made.

d. Regional color differences. Search will be made for regional color differences like those of the lunar maria. Such measurements for Mercury are practically impossible from the earth; a flyby may be able to detect them.

e. Polarization properties of local features. Search will be made to locate any areas of unusually large polarization or those that have albedo-polarization values outside the lunar field.

3. Exploration of Venus

Flyby imagery will attempt to make contributions in the following categories:

a. Clouds. Form and time-dependent properties of the ultraviolet clouds will be investigated. Both vertical structure (from limb and, if possible, cusp observations) and horizontal structure will be considered. It is important to locate the altitude of the ultraviolet markings and to ascertain their relationship to the visible clouds and their lifetimes and velocity relative to the planet. High-resolution overlapping terminator imagery of the main clouds will be investigated as an indicator of their nature and structure. This latter study may have important input to such questions as:

(1) Are the clouds composed of windblown surface particles or atmospheric products?

(2) Are there breaks in the clouds revealing multiple cloud layers?

(3) Are there any cloud manifestations of the infrared emission anomaly near the South Pole or the permanent radar features of the surface?

b. Atmospheric circulation. General characteristics of the atmospheric circulation will be investigated from motion of UV markings, and possibly by inference from large and small scale cloud patterns observable in other spectral regions at higher surface resolution than obtainable from earth.

c. Dark-side optical phenomenon. The possible existence of near ultraviolet and visible airglow emissions (steady or transitory) by imagery of the dark limb in near encounter will be searched.

4. Interplanetary Measurements

Two possibilities are listed here in order that the potentialities of such observations are not ignored in the preliminary design. They would be pursued, if at all,

with the camera system designed for Mercury use, but operated in some long-exposure mode. They are:

(1) To search for satellites of Mercury and Venus. (The present earth-based limit for such objects may be subject to improvement because of the difficulties inherent in viewing Venus, and especially Mercury, so close to the direction of the sun).

(2) To search for minor planets near the sun.

5. In-Flight Calibration and Test Observations

In-flight calibration pictures will be obtained during the near-earth, post-Venus, pre-Mercury, and post-Mercury phases of the mission. The objective of these measurements will be to fully characterize the cameras for photometric and colormetric data reduction. In addition, full-disk high-resolution imagery of the earth and moon will be taken for later comparison of similarly acquired pictures of Venus and Mercury. High-resolution imagery of the lunar terminator will be valuable in order to obtain the optimum predicted exposures for the expected large brightness variations near the terminator of Mercury. These pictures will be used for later comparison of crater counts with similar scale and lighting conditions. Therefore, it is highly desirable to launch during the last quarter of lunar phase.

In-flight star photography will be obtained for intensity and geometric system calibrations.

6. Television Subsystem

In support of the visual imaging experiment, JPL will develop the television instrument. This instrument design will be identical to the design developed and used for the *Mariner* Mars 1971 imaging experiment. It consists basically of two separate camera heads, each containing a vidicon image sensor, its attendant electronics, and independent telescopic optical systems with companion shutter and filter mechanisms.

The twin cameras will have identical optics with a field of view of ⅓ by ½ deg with 1500-mm focal lengths. Each camera will be equipped with a filter wheel that can be controlled to provide any one of several filters in the optical path. The wheel can be advanced in several modes, including one step, two steps, or no steps between consecutive pictures by ground command. An automatic mode may be designed for various strategies at Mercury and Venus.

The *Mariner* Mars 1971 television subsystem is a second generation of the camera systems flown on *Mariner VI* and *VII*. The principal changes in subsystem design from the *Mariner VI* and *VII* subsystems are in adapting to the all-digital data storage subsystem for *Mariner* Mars 1971, increased flexibility of shutter control and filter selection to adapt to the orbital mission, and minor modifications of the detailed design to increase the instrument reliability.

b. Instrument description. Both cameras have focal-plane shutters like those used on the *Mariner* Mars 1971 television cameras. After passing through the filter and shutter, the optical image is focused onto a slow-scan vidicon. Vidicon electron beam focus, alignment, and vertical and horizontal deflection are performed magnetically. See Table 1 for some of the significant instrument parameters.

Table 1. Television subsystem functional parameters

Characteristic	Cameras A and B
Focal length	1500 mm
Focal length ratio	f/7 to f/11 (to be determined)
Nominal shutter operation	3 msec to 6 sec
Long-exposure operation	(To be determined)
Angular field of view	0.48 × 0.37 deg
Active vidicon target raster	9.6 × 12.5 mm
Scan lines per frame	700
Frame time	42 sec
Picture elements per line	832
Pixels/frame	582, 400
Bits per picture element	8
Bits/frame	4, 379, 200
Video carrier frequency	28.8 kHz
Video baseband	7.35 kHz
Video sampling frequency	14.7 kHz
Angle subtended by TV line	9 μrad
Nyquist frequency	33 line pairs/mm horizontal 36 line pairs/mm vertical
Overall system resolution (including optics and electronics)	10% Response at 32 lp/mm

The video information is processed by the signal chain which is shown schematically in Fig. 1. It consists of an ac coupled video amplifier containing a fourth-order bandpass filter, a synchronous demodulator, followed by

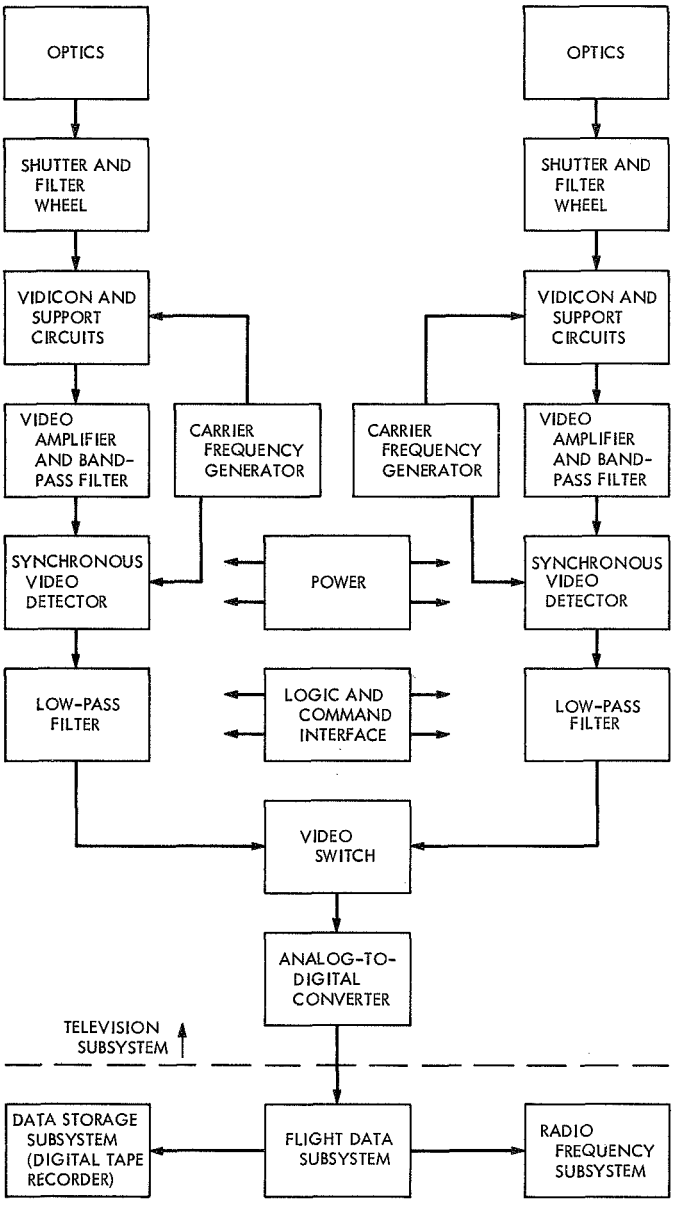

Fig. 1. *Mariner* Venus-Mercury 1973 television subsystem signal flow chart

a fifth-order Butterworth low-pass filter. The video signal from the vidicon is converted to a modulated carrier signal by chopping the vidicon cathode current at the carrier frequency rate. The carrier frequency is 28.8 kHz and is synchronized with the spacecraft power frequency. Some noise rejection is accomplished by phasing the carrier so that the vidicon beam current is off during the switching noise burst generated by the spacecraft primary ac power. The low-pass filter has a bandwidth from dc to 7.35 kHz. The output of this filter is sampled by an 8-bit analog/digital converter at a 14.7-kHz sampling rate which provides a data stream from the TV subsystem of 832 8-bit words for each of the 700 lines comprising one TV frame. The bandpass filter consists of two second-order sections with a bandwidth of 28.8 $\pm$ 7.35 kHz.

The first section of the bandpass filter along with the preamplifier and postamplifier are contained in the camera head. Their function is to provide sufficient gain to raise the video signal from a maximum of about 5 nA obtained from the target electrode in the vidicon to a maximum of 5 V at the camera head output. The first section of the bandpass filter provides noise rejection in the camera head by limiting the signal chain bandwidth. The remainder of the video chain is contained within Bay VII of the spacecraft bus. The bus electronics consists of an ac isolation amplifier to provide common mode noise rejection at the input, the second section of the bandpass filter, the synchronous demodulator, low-pass filter, and analog/digital converter.

The digital signal is transmitted to the flight data subsystem (FDS), where it is rate-buffered and formatted. The formatted data is then routed to the digital tape recorder (DTR) in the data storage subsystem (DSS). In addition, it can be routed to the radio subsystem for real-time transmission or to both the DSS for storage and the radio subsystem for simultaneous transmission.

In order to take advantage of the channel capacity available for data transmission at Mercury and Venus, the *Mariner* Venus–Mercury 1973 spacecraft will have the capability of sending back the television data in quasi-real time. The television data will be compressed in the FDS to match the available S-band channel capacity at Mercury encounter.

7. Preliminary Mission Sequence

This preliminary mission sequence is presented below in the chronological order in which it would be carried out. The experimental objectives for each distinct phase are listed for convenience.

a. Observations in the vicinity of the earth–moon system. A limited number of pictures should be taken and read out soon after launch. These early pictures will test the imaging system prior to the critical points in the mission and provide in-flight calibration data on the system. The pictures required during this phase are:

(1) The full disk of the moon for later comparison with pictures of Venus and Mercury.

(2) The full disk of the earth–moon system for similar comparison purposes and for photometric calibration of the system.

(3) A suitable star field for in-flight geometric calibration of the system.

(4) High resolution pictures of the lunar terminator for experience with large brightness gradients.

Ground resolution in these pictures is to be comparable to at least the late far-encounter portion of the Mercury images. The filters will be visible principally; however, checks on the exposure characteristics of the filters will be made.

b. Cruise observations between earth and Venus. The experimental objectives for this phase of the mission are similar to those listed above. Images of the earth and stars will constitute an in-flight calibration of both the television subsystem and the scan platform.

c. Pre-encounter at Venus. There is little chance for successful experiments at far pre-encounter of the mission due to unfavorable viewing of the planet and the necessity for pointing the camera very nearly in the solar direction. At near pre-encounter, the same difficulties still apply, but there may be the possibility of observing airglow on the dark side of the planet. It may also be possible to observe some detail in the twilight cusp. A resolution of 1 to 2 km with a 1000-km field of view is needed. Ultraviolet and visible filters will be used.

d. Encounter at Venus. Many pictures of the terminator should be taken at Venus encounter. These may reveal small-scale structures, both vertical and horizontal, in the visible clouds. Maximum coverage with stereo overlap should be attempted. The resolution will be 1 km or better. A visible filter will be used.

A preliminary detailed sequence at Venus encounter has been designed for mission planning. This sequence takes advantage of the high data rates and full-resolution pictures will be sent back in the real-time mode every 42 sec. A trajectory plot showing the viewing constraints at Venus are illustrated in Fig. 2.

e. Near post-encounter at Venus. A number of pictures of the limb should be taken during this period. These pictures may distinguish UV from visible clouds. These cloud layers may be separated vertically by as much as 40 km. The resolution will be 1 to 2 km; up to 1000-km dimension may be needed. The filters will be ultraviolet, visible, red, and polarizers. The ultraviolet and visible images must overlap in part.

f. Far post-encounter at Venus. A series of pictures of the entire bright disk should be taken during this period. These pictures would be used to study the apparent motion of the ultraviolet cloud layer. The limb and a significant fraction of the disk should be included in these frames as a reference line. The resolution will be better than 250 km at maximum distance. The filters will be ultraviolet, visible, and polarizer.

g. Cruise observations between Venus and Mercury. In addition to a repetition of the in-flight calibration, it may be desirable to attempt a search for undetected satellites of Venus and especially Mercury. Such observations probably would involve long-exposure pictures of the space adjacent to each planet near the plane of the ecliptic.

h. Far pre-encounter at Mercury. Series of pictures beginning with a resolution of 750 km should be taken during this period. These pictures are needed for:

(1) Comparison with earth-based pictures at the same resolution.

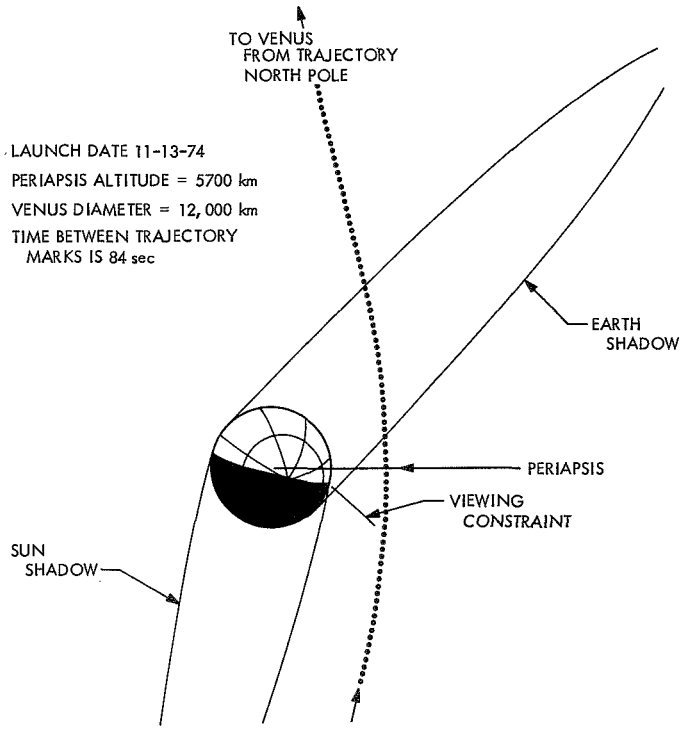

Fig. 2. Viewing constraints of Venus from trajectory North Pole

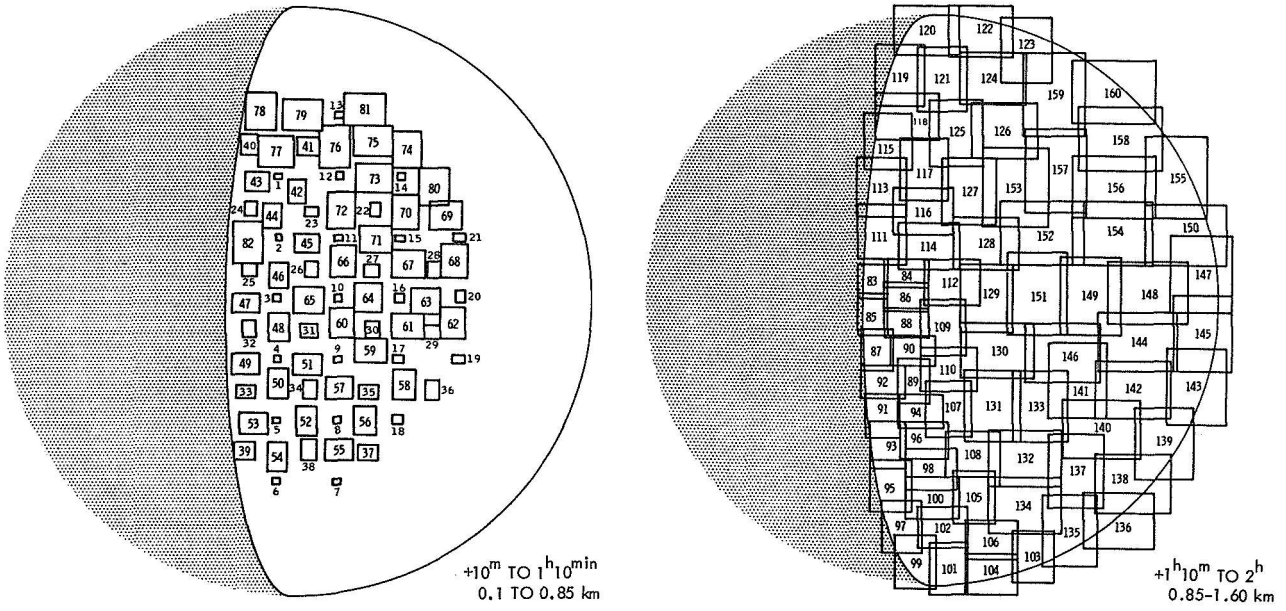

Fig. 3. Typical Mercury sequence (outgoing aspect, one picture every 42 sec)

(2) Determination of spin-axis orientation.

(3) Determination of proper exposure for subsequent pictures.

(4) Coverage of most of the planet's surface area.

The filters will be primarily visible, some red, ultraviolet, and polarizers.

i. Near pre-encounter at Mercury. This is the most important phase of the mission, and the maximum number of pictures should be taken. Maximum coverage at high resolution is needed to reveal small-scale detail on the surface, especially near the terminator. The resolution will be from 10 to 0.1 km; the filters will be primarily visible, some red, ultraviolet, and polarizers.

j. Encounter at Mercury. A preliminary Mercury sequence has been designed for mission planning. This sequence takes advantage of the data compression scheme in the flight data subsystem, which allows complete planet coverage at a surface resolution of 2 to 4 km by mosaicking the pictures. In Fig. 3 the type of coverage possible is illustrated for the data obtained in real-time in this compressed mode on the outgoing trajectory from Mercury. A trajectory plot showing the viewing constraints at Mercury is illustrated in Fig. 4.

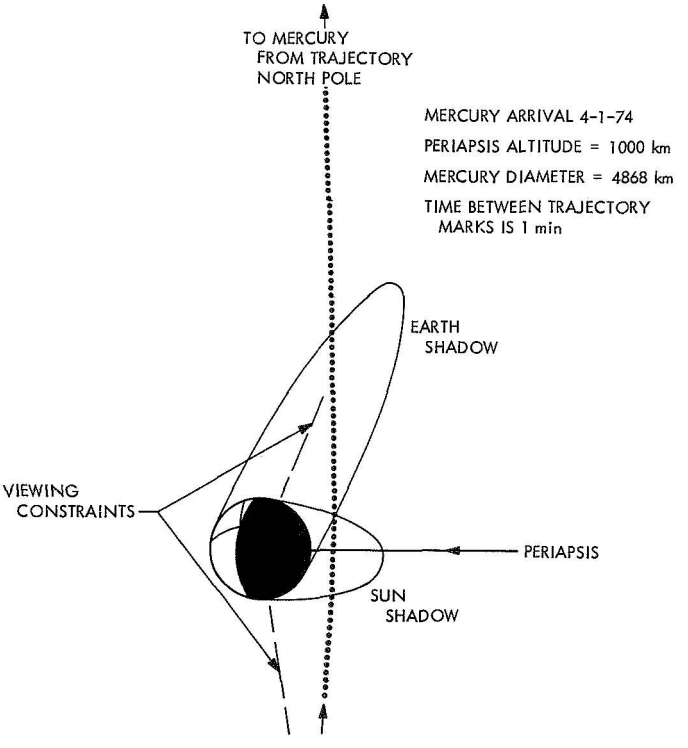

Fig. 4. Viewing constraints of Mercury from trajectory North Pole

k. Near post-encounter at Mercury. The experimental objectives for this part of the mission are identical to those listed for near pre-encounter of Mercury. The only difference is that a new area of the planet will be covered.

l. Far post-encounter at Mercury. The experimental objectives for this part of the mission are identical to those listed for far pre-encounter at Mercury.

m. Post-Mercury cruise observations. The experimental objectives for this part of the mission are similar to those between Venus and Mercury. The geometrical calibration with the star field especially should be repeated. Also, it may be desirable to search for minor planets of the sun at this point, because higher risk spacecraft operations might be possible, such as steering off sun-lock on gyros to provide the extreme cone-angle coverage (for a three-axis stabilized spacecraft).

n. Extended mission. One or two Mercury returns would be extremely beneficial for the imaging experiment by allowing one of the passes to be more nearly optimum for viewing conditions. On a second encounter a polar pass (near the terminator) trajectory would be desirable such that the spacecraft passing distance is no less than 5000 km (in order to obtain photos without smear). On the basis of examining the first set of TV pictures, it is possible that a decision to return to the same point would be made to examine observed features or ambiguities. Furthermore, this return would permit some detailed high-resolution stereo or color pictures to be made on areas suggested by interpretation of the first set of pictures. Any overlap of pictures from two encounters will provide an accurate spin period measurement. The third Mercury encounter could possibly be a polar pass over the opposite pole, i.e., the second Mercury return over the north pole and the third Mercury return over the South Pole.

C. Error Rates for Data Words Time Multiplexed Onto 6-Bit Block-Coded Words, *Spacecraft Telecommunications Systems Section*

1. Introduction

The *Mariner* Mars 1971, *Mariner* Venus–Mercury 1973, and *Viking* (1975) spacecraft communications systems will all have plans to use science data words whose lengths are different from the 6-bit block coded words which will be transmitted over the spacecraft-to-earth communication links received with the multi-mission telemetry system of the DSN. An analysis is presented which shows the error rate for the data words of various word lengths when the error rate for 6-bit coded words is known. No attempt is made to evaluate the gain or loss in information due to quantizing analog data into longer data words having a higher word error rate.

The science words of length M bits are assumed to be serially time multiplexed into 6-bit words. These 6-bit words are mapped into (32,6) biorthogonal coded words and transmitted from the spacecraft to earth. The 6-bit coded words are received, block decoded, and then the science words are decommutated from the received serial bit stream.

2. Mathematical Model

Consider the situation where two or more code words overlap one data word, as in Fig. 1. We define the following events:

α_k = a bit error occurs in at least one of the last k bits of a code word

β_ℓ = a bit error occurs in at least one of the first ℓ bits of a code word

μ = the first overlapping code word is in error

η = the second overlapping code word is in error

γ = a third overlapping code word is in error

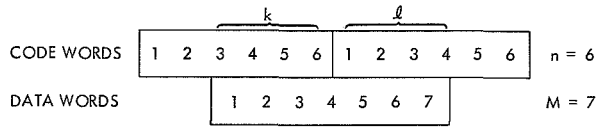

Fig. 1. Case where one 7-bit data word is overlapped by two 6-bit code words

$X(k, \ell)$ = an error occurs in a data word overlapped by k bits of the first code word and ℓ bits of the second.

$X(k, n, \ell)$ = an error occurs in a data word overlapped by k bits of the first code word, an entire n-bit code word, and ℓ bits of the third code word.

Let the probability of an event occurring be denoted by $p(\cdot)$. Then

$$p(x) = p(\alpha_k) + p(\beta_\ell) - p(\alpha_k \cap \beta_\ell) \tag{1}$$

is the probability of error when two code words overlap one data word. Similarly, if three code words n bits long overlap a single data word, then

$$p(x) = p(\alpha_k) + p(\alpha_n) + p(\beta_\ell) - p(\alpha_k \cap \alpha_n) - p(\alpha_k \cap \beta_\ell) - p(\alpha_n \cap \beta_\ell) + p(\alpha_k \cap \alpha_n \cap \beta_\ell) \tag{2}$$

Next, we assume that the presence or absence of an error in one code word is statistically independent from the presence or absence of an error in any other code word. Then

$$p(\alpha_k) = p(\alpha_k|\mu)\, p(\mu) \tag{3}$$

$$p(\beta_\ell) = p(\beta_\ell|\eta)\, p(\eta) \tag{4}$$

$$p(\alpha_k \cap \beta_\ell) = p(\alpha_k)\, p(\beta_\ell) \tag{5}$$

Define ϵ_c as the word error rate of the code words. If ϵ_c is independent of time, then

$$p(\mu) = p(\eta) = \epsilon_c \tag{6}$$

Thus

$$p(x) = \left[p(\alpha_k|\mu) + p(\beta_\ell|\eta)\right] \epsilon_c - \left[p(\alpha_k|\mu)\, p(\beta_\ell|\eta)\right] \epsilon_c^2 \tag{7}$$

when two code words overlap, or

$$p(x) = \left[p(\alpha_k|\mu) + p(\alpha_n|\eta) + p(\beta_\ell|\gamma)\right] \epsilon_c - \left[p(\alpha_k|\mu)\, p(\alpha_n|\eta) + p(\alpha_k|\mu)\, p(\beta_\ell|\gamma) + p(\alpha_n|\eta)\, p(\beta_\ell|\gamma)\right] \epsilon_c^2 + p(\alpha_k|\mu)\, p(\alpha_n|\mu)\, p(\beta_\ell|\gamma)\, \epsilon_c^3 \tag{8}$$

when three code words overlap.

3. Conditional Probabilities

In a (32,6) biorthogonally coded word, up to 7 symbol errors can be made in the code word, and the decoder will still decode the transmitted word. If 8 symbol errors occur, correct detection is uncertain. If 9 to 25 symbol errors are made, the decoder will equally likely map the transmitted word into any of the remaining words in the dictionary except the conjugate of the transmitted word. If more than 25 symbol errors are made, the transmitted word will be mapped into its conjugate. We now make the following approximation: Given that a word error occurs, the transmitted word will equally likely be mapped into any of the remaining words in the dictionary *except* its conjugate.

We are now in a position to construct the conditional probabilities of *Subsection 2*.

Let q_r^n = probability that r successive bits in n bits are all correct, given that the n bit word is in error. Now, there are $2^n/2^r$ words with r specific bits the same in a dictionary of 2^n possible words. The transmitted word can map into $[2^{(n-r)} - 1]$ words having r specific bits the same. There are $(2^n - 2)$ words in the dictionary less the transmitted word and its conjugate. Thus,

$$q_r^n = \frac{2^{(n-r)} - 1}{2^n - 2} \tag{9}$$

For a 6-bit code word,

$$q_r^6 = \frac{\frac{64}{2^r} - 1}{62}$$

Let p_r^n = probability that at least one of r successive bits in n bits is in error, given that the n bit word is in error.

Then

$$p_r^n = 1 - q_r^n \tag{10}$$

Thus

$$p(\alpha_k|\mu) = p_k^n \tag{11}$$

$$p(\beta_\ell|\eta) = p(\beta_\ell|\gamma) = p_\ell^n \tag{12}$$

Table 1 lists p_r^6 for $1 \leq r \leq 6$.

4. Synchronization of Code Words and Data Words

When a data word is mapped onto a code word, there are 6-bit positions of the code word at which the data word may begin. The synchronization chart of Fig. 2 shows these six positions, and labels them A through F. Now a data word M bits long will be mapped in a specific way onto a 6-bit coded word. How the data word is mapped depends on its initial state of synchronization with the code word. For instance, when $M = 2$, there are two unique ways to synchronize. As shown in Fig. 2, either three 2-bit data words are completely contained in one coded word, or 2 data words overlap a coded word, and two are imbedded in the coded word. Figure 2 shows all of the possible sync schemes for mapping M bit data words ($1 \leq M \leq 12$) into 6-bit coded words. The sync cycles are identified by the bit starting positions of the data words.

It should be noted that for those words with more than one unique sync position, that once a serial data stream starts mapping into code words, a sync position will be established and will remain in that sync sequence until the data stream is interrupted, as long as the data word length remains constant. If the data word length of interest changes in the data stream, the mapping of M bit data words onto N bit code words may become asynchronous.

5. Data Word Error Probabilities

Once a synchronization scheme for mapping an M bit data word onto an N-bit coded word is established, the probability of data word error is uniquely determined by the probability of coded word error. Using the notation of *Subsections* 2 and 3, the probability of a data word error can be computed from Eqs. 7, 8, 11, and 12.

As an example, consider the case when $M = 3$. There are three possible sync schemes. The data words either repeat in bit positions ADADAD . . . , BEBEBE . . . , or CFCFCF . . . . When the 3-bit data word is in bit position A, its probability of error is given by $p_3^6\epsilon_c$. When the data word is in bit position D, its probability of error is also $p_3^6\epsilon_c$. A and D occur equally often, so the probability of error for ADAD . . . is $\epsilon_D = p_3^6\epsilon_c$.

Table 1. Conditional probability of an error somewhere in r specific bits given an error in a 6-bit word

r	P_r^6
1	31/62
2	47/62
3	55/62
4	59/62
5	61/62
6	1

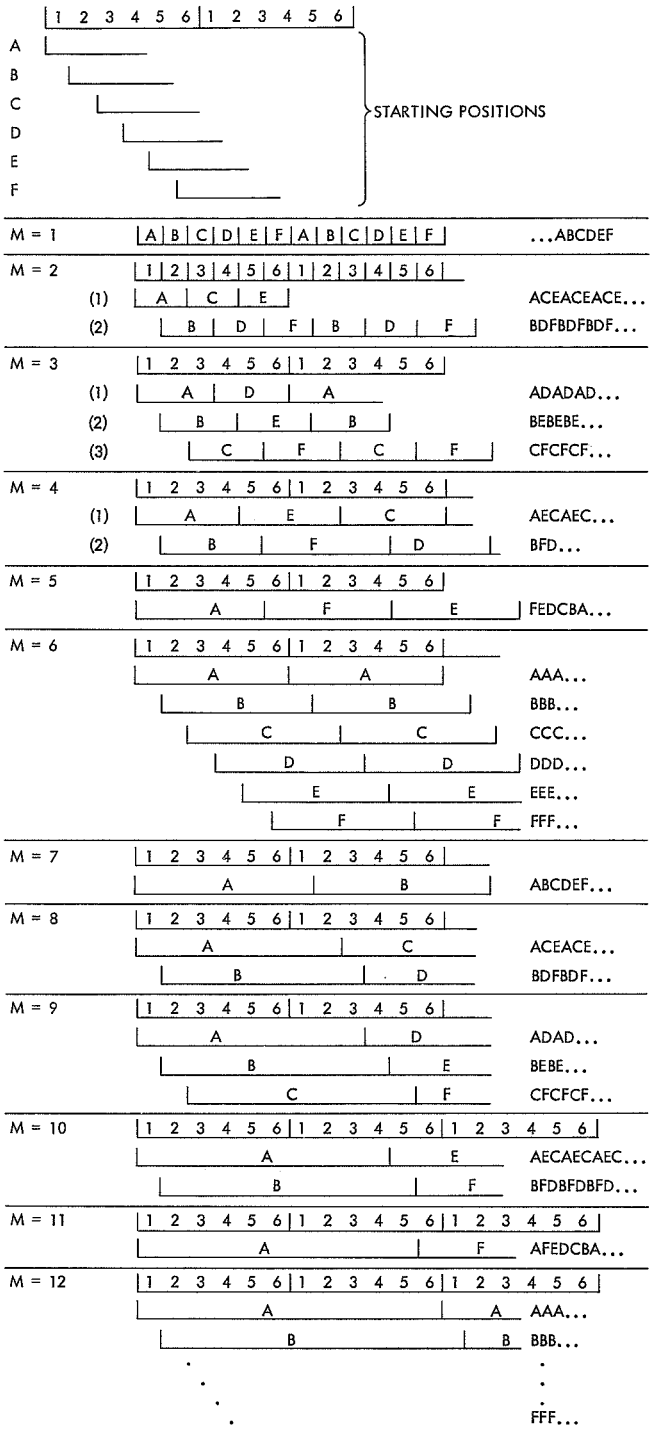

Fig. 2. Synchronization chart

Table 2. Error probability chart[a]

M	Sync	Error rate, ϵ_D
1	1	$p_1\epsilon_c$
2	1	$p_2\epsilon_c$
	2	$1/3\ p_1\epsilon_c + 2/3\ \{2p_1\epsilon_c - (p_1\epsilon_c)^2\} = 5/3\ p_1\epsilon_c - 2/3\ (p_1\epsilon_c)^2$
3	1	$p_3\epsilon_c$
	2	$1/2\ p_3\epsilon_c + 1/2\ [p_1\epsilon_c + p_2\epsilon_c - p_1p_2\epsilon_c^2]$
	3	Same as sync 2
4	1	$2/3\ p_4\epsilon_c + 1/3\ [2p_2\epsilon_c - (p_2\epsilon)^2]$
	2	$1/3\ p_4\epsilon_c + 2/3\ [p_3\epsilon_c + p_1\epsilon_c - p_3p_1\epsilon_c^2]$
5	1	$1/3\ p_5\epsilon_c + 1/3\ [p_4\epsilon_c + p_1\epsilon_c - p_4p_1\epsilon_c^2] + 1/3\ [p_3\epsilon_c + p_2\epsilon_c - p_3p_2\epsilon_c^2]$
6	1	$p_6\epsilon_c$
	2	$p_5\epsilon_c + p_1\epsilon_c - p_5p_1\epsilon_c^2$
	3	$p_4\epsilon_c + p_2\epsilon_c - p_4p_2\epsilon_c^2$
	4	$2p_3\epsilon_c - (p_3\epsilon_c)^2$
	5	Same as sync 3
	6	Same as sync 2
7	1	$1/3\ [p_6\epsilon_c + p_1\epsilon_c - p_6p_1\epsilon_c^2] + 1/3\ [p_5\epsilon_c + p_2\epsilon_c - p_5p_2\epsilon_c^2] + 1/3\ [p_4\epsilon + p_3\epsilon - p_4p_3\epsilon_c^2]$
8	1	$2/3\ [p_6\epsilon_c + p_2\epsilon_c - p_6p_2\epsilon_c^2] + 1/3\ [2p_3\epsilon_c - (p_3\epsilon_c)^2]$
	2	$1/3\ [2p_4\epsilon_c - (p_4\epsilon_c)^2] + 1/3\ [p_3\epsilon_c + p_5\epsilon_c - p_3p_5\epsilon_c^2]$ $+ 1/3\ [2\ (p_1\epsilon_c) + p_6\epsilon_c - 2p_1p_6\epsilon_c^2 - (p_1\epsilon_c)^2 + (p_1)^2\ p_6\epsilon_c^3]$
9	1	$p_6\epsilon_c + p_3\epsilon_c - p_6p_3\epsilon_c^2$
	2	$1/2\ [p_5\epsilon_c + p_4\epsilon_c - p_5p_4\epsilon_c^2] + 1/2\ [p_2\epsilon_c + p_6\epsilon_c + p_1\epsilon_c - p_2p_6\epsilon_c - p_2p_6\epsilon_c^2 - p_2p_1\epsilon_c + p_1p_2p_6\epsilon_c^3]$
	3	Same as sync 2
10	1	$2/3\ [p_6\epsilon_c + p_4\epsilon_c - p_6p_4\epsilon_c^2] + 1/3\ [2p_2\epsilon_c + p_6\epsilon_c - 2p_2p_6\epsilon_c^2 - (p_2\epsilon_c)^2 + (p_2)^2\ p_6\epsilon_c^3]$
	2	$1/3\ [2p_5\epsilon_c - (p_5\epsilon_c)^2] + 2/3\ [p_3\epsilon_c + p_6\epsilon_c + p_1\epsilon_c - p_3p_6\ \epsilon_c^2 - p_3p_1\epsilon_c^2 - p_6p_1\epsilon_c^2 + p_3p_6p_1\epsilon_c^3]$
11	1	$1/3\ [p_6\epsilon_c + p_5\epsilon_c - p_6p_5\epsilon_c^2] + 1/3\ [(p_4 + p_6 + p_1)\ \epsilon_c$ $- (p_4p_6 + p_4p_1 + p_6p_1)\ \epsilon_c^2 + p_4p_6p_1\epsilon_c^3] + 1/3\ [(p_3 + p_6 + p_2)\ \epsilon_c - (p_3p_6 + p_3p_2 + p_6p_2)\ \epsilon_c^2 + p_3p_6p_2\epsilon_c^3]$
12	1	$2p_6\epsilon_c - (p_6\epsilon_c)^2$
	2	$(p_5 + p_6 + p_1)\ \epsilon_c - (p_5p_6 + p_5p_1 - p_1p_6)\ \epsilon_c^2 + p_5p_6p_1\epsilon_c^3$
	3	$(p_4 + p_6 + p_2)\ \epsilon_c - (p_4p_6 + p_4p_2 + p_6p_2)\ \epsilon_c^2 + p_4p_6p_2\epsilon_c^3$
	4	$(2p_3 + p_6)\ \epsilon_c - [2p_3p_6 + (p_3)^2]\ \epsilon_c^2 + (p_3)^2\ p_6\epsilon_c^3$
	5	Same as sync 3
	6	Same as sync 2

[a]Coded word length m is equal to 6 throughout, so the superscript 6 is implied in the notation p^r.

When the 3-bit data word is in sync position BEBE . . . , the error probability is different from the first case. When the data word starts in position B, the error probability is p_3^6. However, when in position E, the data word overlaps two 6-bit coded words, and the error rate is computed from Eq. (7). Thus, the error probability of a 3-bit data word in bit position E is

$$p_1^6\epsilon_c + p_2^6\epsilon_c - p_1^6 p_2^6\epsilon_c^2$$

Since positions B and E occur equally likely in the sequence BEBEBE . . . , the probability of data word error is given by

$$\epsilon_D = \tfrac{1}{2}\, p_3^6\epsilon_c + \tfrac{1}{2}\left(p_1^6\epsilon_c + p_2^6\epsilon_c - p_1^6 p_2^6\epsilon_c^2\right)$$

The third sync sequence, CFCF . . . , can be shown to have the same error rate as BEBE . . . . If a synchronization is established, the error rate will be that of one of the three possible schemes. If the data words are asynchronous, the error rate for a given word length is some average of the error rates for the possible sync schemes.

Table 2 is an error probability chart. It shows the data word error rate when the code words are 6 bits long and the data words are M bits long ($1 \leq M \leq 12$) for all possible sync schemes shown on in Fig. 2.

6. Effect on Communication Performance

The results of *Subsection 5* are presented in the graph of Fig. 3. This graph shows the relative word error rate, $\epsilon = \epsilon_D/\epsilon_c$, when the coded word length is 6 bits and the data word length is M bits. This graph shows clearly how for a given M, one sync scheme will yield superior performance over other possible schemes. The graph also shows how much additional signal energy per bit is required to improve the science data word error rate so that it is equal to the 6-bit coded word error rate previously required of the communication channel.

Figure 3 does not illustrate the loss in data accuracy due to quantization error as the word length is reduced. This report is limited to illustrating the relation of word error rates for different word lengths and synchronization points, when the basic system block codes words which are 6 bits long.

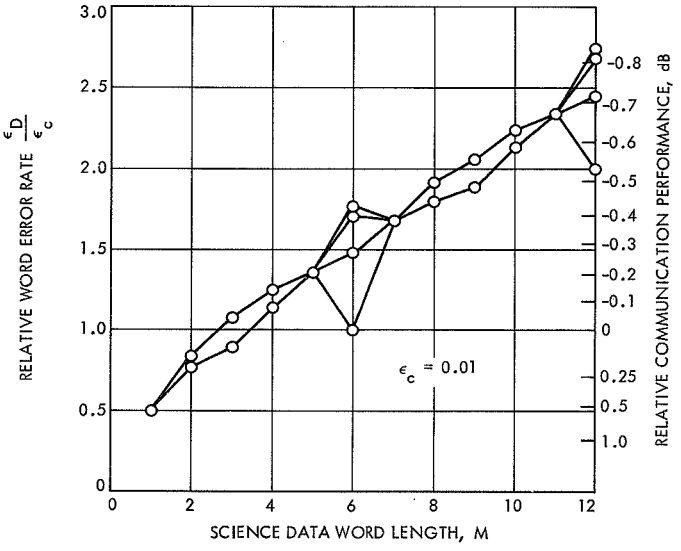

Fig. 3. Science word error rate performance